Pastor-Graells, J., Martins, H.F., Garcia-Ruiz, A., Martin-Lopez, S., Gonzalez-Herraez, M., "Single-shot distributed temperature and strain tracking using direct detection phase-sensitive OTDR with chirped pulses," 2016, Optics Express, Vol. 24, Issue 12, p. 13121-13133

Available at http://dx.doi.org/10.1364/OE.24.013121

Single-shot distributed temperature and strain tracking using direct detection phase-sensitive OTDR with chirped pulses

J. Pastor-Graells,[1,*] H. F. Martins,[2] A. Garcia-Ruiz,[1] S. Martin-Lopez,[1] and M. Gonzalez-Herraez[1]

[1]*Departamento de Electrónica, Universidad de Alcalá, Escuela Politécnica Superior, 28805, Madrid, Spain*
[2]*FOCUS S. L., C/ Orellana, 1, 1° Izquierda, 28804, Madrid, Spain*
[*]*juan.pastor@depeca.uah.es*

Abstract: So far, the optical pulses used in phase-sensitive OTDR (ΦOTDR) were typically engineered so as to have a constant phase along the pulse. In this work, it is demonstrated that by acting on the phase profile of the optical pulses, it is possible to introduce important conceptual and practical changes to the traditional ΦOTDR operation, thus opening a door for new possibilities which are yet to be explored. Using a ΦOTDR with linearly chirped pulses and direct detection, the distributed measurement of temperature/strain changes from trace to trace, with 1mK/4nε resolution, is theoreticaly and experimentaly demonstrated. The measurand resolution and sensitivity can be tuned by acting on the pulse chirp profile. The technique does not require a frequency sweep, thus greatly decreasing the measurement time and complexity of the system, while maintaining the potential for metric spatial resolutions over tens of kilometers as in conventional ΦOTDR. The technique allows for measurements at kHz rates, while maintaining reliability over several hours.

OCIS codes: (060.2370) Fiber optics sensors; (060.2430) Fibers, single-mode; (290.5870) Scattering, Rayleigh.

References and links

1. X. Bao and L. Chen, "Recent progress in distributed fiber optic sensors," Sensors (Basel) **12**(12), 8601–8639 (2012).
2. G. Bolognini, J. Park, M. A. Soto, N. Park, and F. Di Pasquale, "Analysis of distributed temperature sensing based on Raman scattering using OTDR coding and discrete Raman amplification," Meas. Sci. Technol. **18**(10), 3211–3218 (2007).
3. X. Angulo-Vinuesa, S. Martin-Lopez, J. Nuno, P. Corredera, J. D. Ania-Castanon, L. Thevenaz, and M. Gonzalez-Herraez, "Raman-Assisted Brillouin Distributed Temperature Sensor Over 100 km Featuring 2 m Resolution and 1.2 °C Uncertainty," J. Lightwave Technol. **30**(8), 1060–1065 (2012).
4. K. Y. Song, M. Kishi, Z. He, and K. Hotate, "High-repetition-rate distributed Brillouin sensor based on optical correlation-domain analysis with differential frequency modulation," Opt. Lett. **36**(11), 2062–2064 (2011).
5. Y. Peled, A. Motil, and M. Tur, "Fast Brillouin optical time domain analysis for dynamic sensing," Opt. Express **20**(8), 8584–8591 (2012).
6. Y. Peled, A. Motil, I. Kressel, and M. Tur, "Monitoring the propagation of mechanical waves using an optical fiber distributed and dynamic strain sensor based on BOTDA," Opt. Express **21**(9), 10697–10705 (2013).
7. A. Masoudi, M. Belal, and T. P. Newson, "Distributed dynamic large strain optical fiber sensor based on the detection of spontaneous Brillouin scattering," Opt. Lett. **38**(17), 3312–3315 (2013).
8. M. Froggatt and J. Moore, "High-spatial-resolution distributed strain measurement in optical fiber with rayleigh scatter," Appl. Opt. **37**(10), 1735–1740 (1998).
9. B. Soller, D. Gifford, M. Wolfe, and M. Froggatt, "High resolution optical frequency domain reflectometry for characterization of components and assemblies," Opt. Express **13**(2), 666–674 (2005).
10. H. F. Martins, S. Martin-Lopez, P. Corredera, M. L. Filograno, O. Frazão, and M. Gonzalez-Herraez, "Phase-sensitive optical time domain reflectometer assisted by first-order Raman amplification for distributed vibration sensing over >100km," J. Lightwave Technol. **32**(8), 1510–1518 (2014).
11. H. F. Martins, S. Martin-Lopez, P. Corredera, J. D. Ania-Castanon, O. Frazao, and M. Gonzalez-Herraez, "Distributed Vibration Sensing Over 125 km With Enhanced SNR Using Phi-OTDR Over a URFL Cavity," J. Lightwave Technol. **33**(12), 2628–2632 (2015).

#259636 Received 18 Feb 2016; revised 22 May 2016; accepted 23 May 2016; published 7 Jun 2016

12. Z. N. Wang, J. Li, M. Q. Fan, L. Zhang, F. Peng, H. Wu, J. J. Zeng, Y. Zhou, and Y. J. Rao, "Phase-sensitive optical time-domain reflectometry with Brillouin amplification," Opt. Lett. **39**(15), 4313–4316 (2014).
13. Z. N. Wang, J. J. Zeng, J. Li, M. Q. Fan, H. Wu, F. Peng, L. Zhang, Y. Zhou, and Y. J. Rao, "Ultra-long phase-sensitive OTDR with hybrid distributed amplification," Opt. Lett. **39**(20), 5866–5869 (2014).
14. F. Peng, H. Wu, X. H. Jia, Y. J. Rao, Z. N. Wang, and Z. P. Peng, "Ultra-long high-sensitivity Φ-OTDR for high spatial resolution intrusion detection of pipelines," Opt. Express **22**(11), 13804–13810 (2014).
15. A. Masoudi, M. Belal, and T. P. Newson, "A distributed optical fibre dynamic strain sensor based on phase-OTDR," Meas. Sci. Technol. **24**(8), 085204 (2013).
16. Z. Wang, L. Zhang, S. Wang, N. Xue, F. Peng, M. Fan, W. Sun, X. Qian, J. Rao, and Y. Rao, "Coherent Φ-OTDR based on I/Q demodulation and homodyne detection," Opt. Express **24**(2), 853–858 (2016).
17. G. Tu, X. Zhang, Y. Zhang, F. Zhu, L. Xia, and B. Nakarmi, "The Development of an Phi-OTDR System for Quantitative Vibration Measurement," IEEE Photonics Technol. Lett. **27**(12), 1349–1352 (2015).
18. H. F. Martins, S. Martin-Lopez, P. Corredera, M. L. Filograno, O. Frazão, and M. Gonzalez-Herraez, "Coherent Noise Reduction in High Visibility Phase-Sensitive Optical Time Domain Reflectometer for Distributed Sensing of Ultrasonic Waves," J. Lightwave Technol. **31**(23), 3631–3637 (2013).
19. Z. Qin, L. Chen, and X. Bao, "Wavelet denoising method for improving detection performance of distributed vibration sensor," IEEE Photonics Technol. Lett. **24**(7), 542–544 (2012).
20. Y. Koyamada, M. Imahama, K. Kubota, and K. Hogari, "Fiber-Optic Distributed Strain and Temperature Sensing With Very High Measurand Resolution Over Long Range Using Coherent OTDR," J. Lightwave Technol. **27**(9), 1142–1146 (2009).
21. L. Zhou, F. Wang, X. Wang, Y. Pan, Z. Sun, J. Hua, and X. Zhang, "Distributed Strain and Vibration Sensing System Based on Phase-Sensitive OTDR," IEEE Photonics Technol. Lett. **27**(17), 1884–1887 (2015).
22. M. A. Soto, X. Lu, H. F. Martins, M. Gonzalez-Herraez, and L. Thévenaz, "Distributed phase birefringence measurements based on polarization correlation in phase-sensitive optical time-domain reflectometers," Opt. Express **23**(19), 24923–24936 (2015).
23. L. B. Liokumovich, N. A. Ushakov, O. I. Kotov, M. A. Bisyarin, and A. H. Hartog, "Fundamentals of Optical Fiber Sensing Schemes Based on Coherent Optical Time Domain Reflectometry: Signal Model Under Static Fiber Conditions," J. Lightwave Technol. **33**(17), 3660–3671 (2015).
24. H. F. Martins, J. Pastor-Graells, L. R. Cortés, D. Piote, S. Martin-Lopez, J. Azaña, and M. Gonzalez-Herraez, "PROUD-based method for simple real-time in-line characterization of propagation-induced distortions in NRZ data signals," Opt. Lett. **40**(18), 4356–4359 (2015).
25. F. Li, Y. Park, and J. Azaña, "Complete temporal pulse characterization based on phase reconstruction using optical ultrafast differentiation (PROUD)," Opt. Lett. **32**(22), 3364–3366 (2007).
26. J. Azaña, Y. Park, and F. Li, "Linear self-referenced complex-field characterization of fast optical signals using photonic differentiation," Opt. Commun. **284**(15), 3772–3784 (2011).
27. H. F. Martins, S. Martin-Lopez, P. Corredera, P. Salgado, O. Frazão, and M. González-Herráez, "Modulation instability-induced fading in phase-sensitive optical time-domain reflectometry," Opt. Lett. **38**(6), 872–874 (2013).

1. Introduction

Distributed Optical Fiber Sensors (DOFS) allow for the continuous measurement of different physical parameters (temperature, strain, birrefringence) over long fiber distances and therefore provide a cost-effective solution for the monitoring of large civil infrastructures such as bridges, tunnels, pipelines or railways. DOFS are based on Rayleigh, Brillouin or Raman scattering phenomena, which depend on strain, temperature or birrefringence changes within the optical fiber [1].

Using Raman-based sensing for static measurements, spatial/temperature resolutions of 17m/5K have been demonstrated over 40 km [2] with measurement times of a few minutes. With traditional Brillouin Optical Time Domain Analysis (BOTDA), spatial/temperature resolutions of 2m/1.2K over 100 km have been demonstrated [3], but, due to the requirement of a large of number averages and a frequency sweep, the measurement times are still typically of several minutes. Recently, schemes using Brillouin based sensing have been proposed for dynamic strain sensing [4–7]. In 2011, samplings of 20 Hz were demonstrated in a version of Brillouin optical correlation-domain analysis (BOCDA) [4]. However typically the range is quite limited in this type of sensors. With a fast implementation of BOTDA [5], samplings of 10 kHz with a standard deviation of strain of 5με were demonstrated, although the technique was best suited for short fibers (100 meters in [5]) and a low number of averages, as a frequency sweep was still required. The same group later demonstrated a practical utilization of the slope-assisted BOTDA to allow for strain measurements without requiring a frequency sweep [6]. In this case, the dynamic response is achieved by working tuned to the slope of the Brillouin gain response of the fiber. The proposed technique

#259636 Received 18 Feb 2016; revised 22 May 2016; accepted 23 May 2016; published 7 Jun 2016

presented several limitations when compared to the conventional BOTDA, particularly concerning the strain dynamic range, which is limited by the width of the Brillouin gain spectrum of the tested fiber. BOTDR implementations also allow to do dynamic strain measurements over 2 km [7] with an accuracy of 50 με and spatial resolution of 1.3 m. However, sampling ratios higher than few Hz have not been achieved.

As for Rayleigh-based sensing, it typically requires lower averaging than Raman or Brillouin, and is therefore better suited for dynamic measurements. In the frequency domain, optical frequency domain reflectometry (OFDR) can provide high spatial resolutions [8,9], but is typically limited to short fiber sections due to the sweeping laser requirements. As for measurements in the time domain, the feasibility of phase-sensitive optical time domain reflectometry (ΦOTDR) to be used for sensing with spatial resolutions of a few meters over distances which can go well above 100 km has been well estabilished [10–14]. However, true strain/temperature readings cannot be performed with this system unless complex phase recovery methods are deployed [15–17].

On the one hand, traditional ΦOTDR (without phase recovery) allows for distributed vibration measurements with a high bandwidth, only limited by the fiber length, ranging from 10's of kHz for a few kilometers [18,19], to 100's of Hz for more than 100 km [10–14]. These measurements however, are based on intensity variations of the ΦOTDR signal which does not show a linear variation with the applied perturbation. On the other hand, by precisely sweeping the frequency of the pulses step by step, ΦOTDR has been shown to allow for very sensitive static measurements of refractive index variations, which can be used for very high resolution temperature [20], strain [21] and birefringence [22] measurements. For instance, the demonstrated temperature resolutions of 0.01 °C [20] are two orders of magnitude below the typical resolutions of ≈1 °C provided by Brillouin sensors. However, due to the requirements of a frequency scan, in this case the measurement time and complexity of the system is increased.

By recovering the phase of the ΦOTDR signal, the dynamic measurement of strain has been demonstrated [15–17]. In this case however, the system is more complex and laser coherences of at least the fiber length are required in order to avoid noise when beating the signal with the local oscillator. The long term-stability of such systems (i.e. after several minutes or hours) and therefore feasibility for static temperature measurements over several hours has also not been clearly addressed either.

In this paper we provide a method based on ΦOTDR using chirped pulses to allow for the measurement of distributed strain and temperature changes, in a single shot and without the requirement of a frequency scan. The complexity of the system is therefore not significantly increased when compared to traditional ΦOTDR systems using intensity-based detection. With the proposed method, it is possible to combine the best features of ΦOTDR which had been previously demonstrated by separate: on the one hand, fast mesurements with a bandwidth only limited by the fiber length, potentially over several 10's of kilometers with metric spatial resolutions; on the other hand, the measurement of temperature/strain variations with resolutions which can be several orders of magnitude below those provided by Brillouin. Since the measurement is relative, the range of temperature/strain measurements is in principle not limited, being in practice determined by how the cumulative errors of the measurement are handled. The technique allows for measurements at kHz rates, while maintaining reliability over several hours of measurement. The sensitivity can also be tuned by acting on the chirp of the pulses. Temperature/strain resolutions of 1mK/4nε are demonstrated.

2. Traditional ΦOTDR: general concepts

A ΦOTDR is a distributed sensing technique which makes use of the Rayleigh scattering effect and allows for the measurement of perturbations along an optical fiber. In this method, highly coherent optical pulses are injected into an optical fiber. The Rayleigh backscattered light is monitored in the time domain, which is then associated with fiber position using the time of flight of the light pulses in the fiber. As coherent pulses are used, the ΦOTDR signal

#259636 Received 18 Feb 2016; revised 22 May 2016; accepted 23 May 2016; published 7 Jun 2016

will be the result of the coherent interference between the fields which are Rayleigh backscattered from the multiple fiber scattering centers [23]. Ideally, the phase noise existant in the pulses should be kept to a minimum, as it will increase the noise of the ΦOTDR signal. With this in mind, the phase of the optical pulses used in ΦOTDR systems has never been really engineered, as it has always been a priority to keep this phase as flat and constant as possible. The idea in this paper is that a *deterministic* (but non-flat) phase profile in the pulses may be used to render the ΦOTDR implementation more efficient, as we will show below.

The ΦOTDR signal depends on the multiple (random) contributions given by the scattering centers, but also on the intensity and phase profiles of the pulses. Typically, the resulting detected intensity will present a random noise-like shaped pattern. This pattern will remain constant and reproducible if the fiber and measuring conditions do not change over time. Perturbations in the fiber can be detected by monitoring local changes in the ΦOTDR signal with a bandwidth of detection which is only limited by the fiber length [18]. However, it is often hard to precisely quantify the amplitude of the perturbations, as the intensity variations of the ΦOTDR signal do not show a linear correlation with the amplitude of the applied perturbations. Conventional ΦOTDR systems using a single pulse frequency are therefore best suited to detect the frequency of a dynamic perturbation rather than its amplitude, and are most commonly used for vibration/intrusion detection [10–14,18].

While the intensity variations of the ΦOTDR signal cannot be predicted for a given perturbation, the changes in optical path difference between the scattering centers induced by a uniform refractive index change Δn can be compensated by a shift of the pulse frequency Δv, which allows the recovery of the original ΦOTDR pattern. Assuming small refractive index changes ($\Delta n << n$), the necessary Δv to compensate for a given Δn can be derived from [20,22]:

$$\frac{\Delta n}{n} = \frac{\Delta v}{v_0} \tag{1}$$

where v_0 is the central frequency of the pulse and n the effective refractive index of the fiber. Based on this principle ΦOTDR systems have been demonstrated to allow for quantitative measurements of temperature/strain [20] and birefringence [22] with high measurand resolutions. However, in this case, a frequency sweep of the pulse is required, which greatly increases the measurement time, typically up to a few seconds or a few minutes. The system turns out then to present similar tradeoffs to traditional Brillouin temperature sensors, having a temperature resolution and range which is dependent on the used frequency scan step and range. High measurand resolutions over long ranges can therefore be highly time consuming. The maximum achievable resolution is also limited by the pulse spectral content [22], in a somewhat similar manner to the temperature resolution limitation imposed by the spectral width of the Brillouin gain curve in Brillouin sensors.

3. Proposed chirped-pulse ΦOTDR: Theoretical Model

The method proposed in this paper for temperature/strain variation measurements originates from the principle described in (1) that a refractive index change Δn in the fiber can be compensated (in terms of the shape of the trace) by a frequency shift Δv of the pulse sent into the fiber. This is the same principle as used in [20,22], and is typically implemented by performing a laser frequency sweep. In our case, instead of requiring a time-consuming frequency sweep to determine Δv and calculate Δn, a single pulse which has linear chirp is used. Since different positions of the pulse have different frequencies, when a Δn is applied, the same trace pattern at a given position can be generated by a temporally-shifted region of the pulse, leading essentially to a longitudinal shift Δz of the local ΦOTDR trace. It is then possible to calculate Δv (and consecuently Δn and the temperature/strain shift) from Δz, which is obtained directly from the time-domain trace measurements. Thus, in our method, a single trace measurement should be sufficient to determine temperature/strain changes. The theoretical description of the proposed method is presented in detail in this section.

#259636 Received 18 Feb 2016; revised 22 May 2016; accepted 23 May 2016; published 7 Jun 2016

Although it is a general concern in conventional ΦOTDR systems to have flat-phase profiles, it should be clear that the optical pulses used in a ΦOTDR can in principle have any arbitrary phase profile, and therefore any arbitrary spectral content. What is important to avoid additional noise in the trace is that the phase profile does not change from pulse to pulse (i.e. that the master laser has a low phase noise). Therefore, except for the fact that the detection bandwidth should be higher in the case of chirped pulses, no extra noise source should be expected in our implementation over the traditional one, and therefore similar spatial resolutions and sensing ranges should be achievable in both methods. An evaluation of the propagation-induced distortions may be required when operating with pulses with large spectral contents and long fiber distances, mainly due to dispersion. Such extensive evaluation is nevertheless out of the scope of this paper. However, using a few tens of kilometers and pulses with spectral contents of up to ≈1 GHz, ΦOTDR operation should not be greatly affected [24].

To describe the proposed ΦOTDR sensor, we start by describing a pulse $P(t,z)$, with a rectangular intensity profile of amplitude E_0, width τ_p and an instantaneous frequency profile $v(t) = v_0 + (\delta v/2 - \delta v \cdot [t/\tau_p])$. $P(t,z)$ is therefore a linearly chirped pulse with a spectral content δv, around a central frequency v_0, and frequency slope $\delta v/\tau_p$. The propagation of $P(t,z)$ along an optical fiber is described by:

$$P(t,z) = E_0 \cdot rect\left[\left(t - \int_0^z n(z)dz/c\right)\Big/\tau_p\right] \cdot e^{i2\pi\left(v_0+\delta v/2-\delta v/\tau_p\cdot\left[t-\int_0^z n(z)dz/c\right]\right)\left(t-\int_0^z n(z)dz/c\right)} \quad (2)$$

where t is the time and z the position along the fiber, $z = 0$ being the fiber entrance where the pulses are lauched and $t = 0$ the moment when the front part of the pulse enters the fiber in $z = 0$. rect(x) = *1* when $0 \le x \le 1$ and zero elsewhere, c is the speed of light in the vacuum and $n(z)$ is the local refractive index of the fiber at the pulse central frequency v_0. The spectral content δv is assumed to be small in comparison to the center frequency and v_0 to be away from resonant frequencies of the fiber, so that the dependency of n in the optical frequency (i.e., dispersion) is negligible. In any case, this dependency can be introduced if a more precise theoretical model is required.

As the pulse $P(t,z)$ propagates along the fiber, at each instant t each infinitesimal part of P will generate a counter-propagating wave via Rayleigh backscattering. The backscattered signal is therefore continuously generated, and different parts of backscattered signals generated at different instants will overlap to produce the ΦOTDR signal $E(t)$, received at $z = 0$, at a given time t.

The reflection of $P(t,z)$ in each location of the fiber z is described by the fiber's Rayleigh backscattering profile function $r(z)$. $E(t)$ will be given by the convolution of $P(t,z)$ and $r(z)$, for the fiber section $z \in [(t-\tau_p)\cdot c/(2n),\ t\cdot c/(2n)]$:

$$E(t) = \int_{z=tc/2n-\tau_p c/2n}^{tc/2n} r(z) \cdot E_0 \cdot e^{i2\pi\left(v_0+\delta v/2-\delta v/\tau_p\cdot\left[t-2\int_0^z n(z)dz/c\right]\right)\left(t-2\int_0^z n(z)dz/c\right)} dz \quad (3)$$

Note that while the signal $E(t)$ is generated from the interference of reflections occurring in a fiber section with ½ of the pulse width, it accounts for the passage of the entire pulse $P(t,z)$. This characteristic is the basis for the well known fact that the spatial resolution for OTDR systems is determined by ½ of the pulse width.

Figure 1 depicts the reflections of the pulse $P(t,z)$ as it propagates along the fiber which will generate $E(t)$. The contribution to $E(t)$ will be given by a convolution of P with the fiber sections $z \in [z_1,z_2],[z_2,z_3]$, which reflect the instantaneous frequencies $v \in [v_4,v_3],[v_3,v_1]$, respectively, as shown in Fig. 1(a). The contribution to $E(t + \Delta t)$ will be given by a convolution of P with the fiber sections $z \in [z_2,z_3],[z_3,z_4]$ which reflect the instantaneous frequencies $v \in [v_4,v_2],[v_2,v_1]$, respectively, as shown in Fig. 1(b). For a small enough Δt, so that $[z_1,z_2],[z_3,z_4] \ll [z_2,z_3]$, then the contributions to $E(t)$ and $E(t + \Delta t)$ generated from reflections in $[z_1,z_2],[z_3,z_4]$ are essentially negligible. In this case, $E(t)$ and $E(t + \Delta t)$ can be

#259636 Received 18 Feb 2016; revised 22 May 2016; accepted 23 May 2016; published 7 Jun 2016

thought of as generated from reflections of the same fiber section $[z_2,z_3]$, by pulses with frequencies $\upsilon \in [\upsilon_3,\upsilon_1]$ and $\upsilon \in [\upsilon_4,\upsilon_2] = [\upsilon_3,\upsilon_1] + \Delta\upsilon$, respectively, i.e., two pulses with a frequency shift $\Delta\upsilon$ between them.

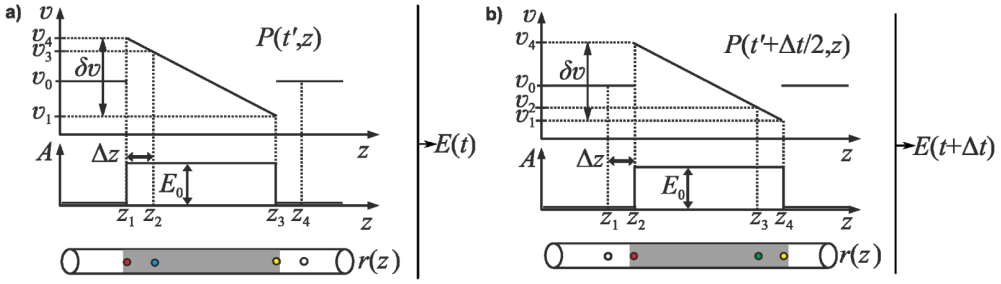

Fig. 1. Reflection of the pulse P(t,z) as it propates along the fiber.

In this case, if n remains constant along $[z_2,z_3]$, then $E(t) \neq E(t + \Delta t)$. However, if a homogeneous Δn occurs, so that the equality of Eq. (1) is verified, then the Δn is compensated by the frequency shift $\delta\upsilon$ and therefore $E(t) = E(t + \Delta t)$. This can be mathematically directly derived from Eq. (3), assuming that the contributions to the integral from $[z_1,z_2]$ (to $E(t)$) and $[z_3,z_4]$ (to $E(t + \Delta t)$) are negligible. In practice, this relation holds if Δn is small enough, as discussed at the end of this section. The relation between these quantities can be derived by analizing the phase difference $\varphi_{i,j}$ between the backscattered waves reflected from the fiber locations z_i,z_j, similarly to what is derived in [20]:

$$\phi_{i,j} = -2\pi \frac{2n(z_i - z_j)}{c}\left(\upsilon_0 + \frac{\delta\upsilon}{2} - \frac{\delta\upsilon}{\tau_p}\cdot\left[2t - \frac{2n(z_i + z_j)}{c}\right]\right) \tag{4}$$

From Eq. (4) it follows that a small variation Δn can be compensated by a longitudinal shift of the trace Δt (after neglecting terms of small amplitude and taking into account a factor of 2 owned to the fact that the pulse is reflected from a fiber section with ½ of the pulse length). The relationship between Δn and Δt is given by:

$$\left(\frac{\Delta n}{n}\right) = -\left(\frac{1}{\upsilon_0}\right)\cdot\left(\frac{\delta\upsilon}{\tau_p}\right)\cdot\Delta t \tag{5}$$

A similar derivation can be done for strain changes, which in addition lead to a change in the relative positions of z_i,z_j. The measuring principle of the proposed chirped-pulse ΦOTDR sensor derives from this result. If a Δn occurs at a certain location of the fiber z, then the local ΦOTDR pattern $E(t)$ will be longitudinaly shifted by a Δt at that location, correspondent to the $\Delta\upsilon$ which compensates for the Δn. Note that local Δt changes among two different traces can be determined along the fiber by calculating a local correlation of the trace segments obtained for the two consecutive measurements.

The measurement of Δn along the fiber then allows for distributed temperature measurements ΔT. A similar derivation can be performed for applied strains $\Delta\varepsilon$, (which are translated into shifts of the scattering positions of the fiber Δz). If a $\Delta\varepsilon$ occurs then E(t) will be longitudinaly shifted by a Δt, which will be added to existing Δt caused by ΔT (if existant). The relation between Δt and the quantities ΔT and $\Delta\varepsilon$ is given by [20]:

$$-\left(\frac{1}{\upsilon_0}\right)\cdot\left(\frac{\delta\upsilon}{\tau_p}\right)\cdot\Delta t = \frac{\Delta\upsilon}{\upsilon_0} \approx -0.78\cdot\Delta\varepsilon \tag{6}$$

$$-\left(\frac{1}{\upsilon_0}\right)\cdot\left(\frac{\delta\upsilon}{\tau_p}\right)\cdot\Delta t = \frac{\Delta\upsilon}{\upsilon_0} \approx -\left(6.92\cdot10^{-6}\right)\cdot\Delta T \tag{7}$$

#259636 Received 18 Feb 2016; revised 22 May 2016; accepted 23 May 2016; published 7 Jun 2016

In this case, the measurement is essentialy continuous, and the minimum detectable Δn is determined by the chirp ($\delta v/\tau_p$) and the sampling (and bandwidth) with which $E(t)$ is detected. For large Δn, the contributions of $[z_1,z_2]$,$[z_3,z_4]$ may become relevant and introduce significant deformations to the ΦOTDR trace, thus limiting the validity of the approach. Experimental results indicate that to ensure correct measurements, the maximum measureable Δn should correspond to a frequency change Δv (Eq. (5) so that $\Delta v/\delta v \approx$2-3%. This imposes a maximum measurable Δt which should correspond to 2-3% of the pulse length (τ_p). Since the measurements can be made quite fast (there is no requirement for a frequency sweep and single-shot acquisitions are perfectly feasible) the expectable changes from trace to trace should be quite small. Measurements of large Δn variations (which typically should take long times to develop) can be also be done, in this case accumulating the measured delay values (Δt) between consecutive traces. In this way, values of Δn which are correspondent to a Δv arbitraly larger than δv can be detected, as long as the errors accumulated between the consecutive measurements are kept small. This allows for fast measurements of temperature or strain, with high resolution and over long ranges, as will be demonstrated in this article.

4. Measuring technique

While traditional ΦOTDR measure intensity variations of all the points of the trace over time, the proposed chirped-pulse ΦOTDR sensor analyses the longitudinal ΦOTDR trace shifts that occur along the fiber. We denote this profile of local trace shift variations as $\Lambda(t)$, which is related to the temperature or strain gradients suffered by the fiber, as discussed in the previous section. The fiber is measured at two different (consecutive) times t_1,t_2, by sending two (equal) pulses P_1, P_2 into the fiber, from which result two traces $E_1(t)$, $E_2(t)$. Note that the ΦOTDR pattern $E(t)$ is associated with a fiber position z, by $t = 2nz/c$. The $\Lambda(t)$ occurred between the $E_1(t)$ and $E_2(t)$ is calculated using a moving window of cross-correlation along $E_1(t)$, $E_2(t)$, defined by a certain correlation time τ_{corr}:

$$\Lambda(t) = \max\left(correlation\left[E_1\left(t-\tau_{corr}, t+\tau_{corr}\right), E_2\left(t-\tau_{corr}, t+\tau_{corr}\right)\right]\right) \qquad (8)$$

Here τ_{corr} should be of the order of τ_p, and will set the spatial resolution. The temperature/strain variations which occurred in the fiber between t_1,t_2, can then be calculated using Eq. (5-7). A continuous measurement of temperature/strain along time is possible by simply integrating the successive measurements obtained for $[E_1(t), E_2(t)]$, $[E_2(t), E_3(t)]$…, $[E_{n-1}(t), E_n(t)]$.

However, a simple analysis will show that this is not the best way to minimize the cumulative errors of a measurement. For very small values of index change, close to the resolution of the sensor (set by the chirp and the sampling of $E(t)$), the error will increase due to quantization error. For large values of index change, the error will increase because the contributions for $E(t)$ generated from $[z_1,z_2]$,$[z_3,z_4]$ (see Fig. 1) are no longer negligible. Therefore, for a certain measurement setup, there will be a certain range of index change values for which the measurement error is minimum. An efficient way of minimizing the error in case of small variations is then to use the measurement of consecutive traces as a first estimate and then compare pairs of $[E_i(t), E_j(t)]$ that are more spaced in time, and for which the calculated temperature/strain variations are close to the shifts where the error is known to be minimum. Other algorithms taking into account multiple comparisons of traces to reduce the measurement error can be thought of.

5. Experimental setup

The experimental setup used to measure temperature/strain changes with the new proposed technique is depicted in Fig. 2. It is based on a traditional ΦOTDR scheme [18] but introducing a linear chirp in the pulse through the current control of the laser.

#259636 Received 18 Feb 2016; revised 22 May 2016; accepted 23 May 2016; published 7 Jun 2016

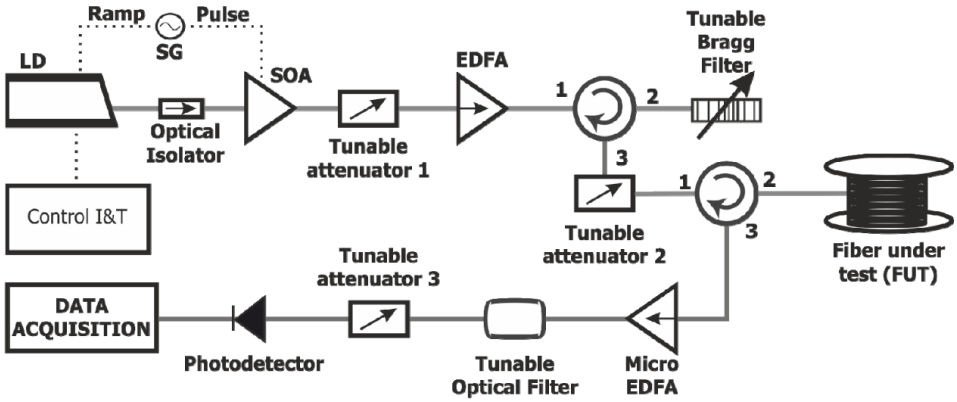

Fig. 2. Experimental setup: acronyms are explained in the text.

The light source was a laser diode (LD) with a linewidth of 1.6 MHz emitting at 1546.66 nm and working in continuous emission. The LD was driven by a standard current and temperature controller to select the laser central wavelength. A secondary current control applied a repetitive electric ramp signal in the laser driver, which introduced a linear chirp at certain times in the outputted laser light. This light was then gated in the time domain by a semiconductor optical amplifier (SOA) – whose driver was synchronized with the secondary laser current control - thus generating linearly chirped pulses. The SOA had rise/fall times in the order of 2.5 ns, and was driven by a waveform signal generator (SG), to create 100 ns square pulses, which implies a spatial resolution of 10 m in this case. An optical isolator was used between the LD and the SOA to avoid laser instabilities due to reflections in the following devices. Three different chirp slopes were applied on the optical pulses, resulting in total pulse spectral contents ranging from 0.8 GHz to 2.3 GHz. To avoid errors, they were characterized experimentally by means of phase reconstruction using optical ultrafast differentiation (PROUD), a self-referenced technique which allows recovering the instantaneous frequency and phase of arbitrary optical signals. Particularly, balanced PROUD has been used in this experiment, which allows obtaining in real-time the instantaneous frequency profile of a pulse [24–26]. The setup for this characterization is exactly the same that was used in a previous work by the same authors [24]. The three chirp slopes induced in the optical pulses are presented in Fig. 3, having the following spectral contents: $Chirp_1$ = 0.81 ± 0.02 GHz (black), $Chirp_2$ = 1.62 ± 0.04 GHz (red) and $Chirp_3$ = 2.32 ± 0.05 GHz (green). The main source of uncertainty in these values was the slope of the optical filter used to derivate the signal [24] which could be at least 1%. An extensive study on the errors introduced on the measurement due to variations of the pulse chirp profile from the ideal linear chirp (used in the theoretical model of section 3) is out of the scope of this paper. In any case, the chirp profile of the pulses showed a good linearity, and should therefore introduce small errors in the temperature/strain measurements.

#259636 Received 18 Feb 2016; revised 22 May 2016; accepted 23 May 2016; published 7 Jun 2016

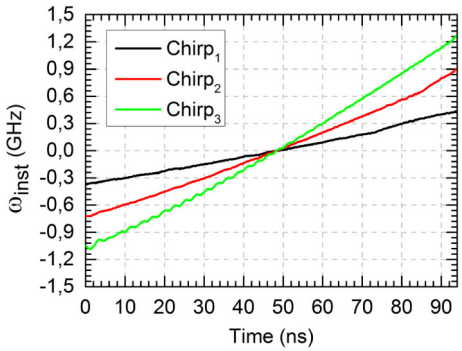

Fig. 3. Instantaneous frequency profile of the three different chirps induced in 100 ns optical pulses.

An erbium-doped fiber amplifier (EDFA) is used to amplify the pulse peak power to achieve longer sensing distances. Between the SOA and the EDFA, a variable optical attenuator is introduced to control the EDFA input power and to avoid possible nonlinearities generated in it. Note that if no nonlinearities occur in the EDFA, this attenuator (attenuator 1) is not required in the setup, since the power of the optical pulse injected into the fiber can be tuned using only attenuator 2. In order to filter the amplified spontaneous emission (ASE) added by the EDFA, a tunable fiber Bragg grating (FBG) working in reflection is inserted. The FBG spectral width is 0.8 nm.

Before injecting the optical pulse in the fiber under test (FUT), another tunable attenuator controls the input power to avoid nonlinearities in the fiber, mainly due to modulation instability (MI) [27]. The backscattered signal is amplified with another EDFA and filtered with a 0.5 nm spectral width optical filter. Finally, the light is detected in a p-i-n photo-detector with a bandwidth of 13 GHz and a high-speed digitizer with 40 GHz sampling rate. Furthermore, to avoid damaging the p-i-n photodetector, another tunable attenuator controls its input power. Note that, in comparison with traditional ΦOTDR systems, here the detection bandwidth and digitizing speed need to be much higher, as they should cover the total bandwidth of the chirp signal used.

The FUT used in the experiment has a length of 1 km. All the FUT is immersed in a water bath, to maintain the fiber temperature stable. For the temperature meassurements, the last 20 m of the FUT were placed inside an oven which allowed to control the temperature. The temperature inside de oven is registered with a thermometer with a resolution of 0.1 °C, for a later comparison with the fiber measurements. For the strain measurements, the last 20 m of the FUT were strapped around a PZT which allowed the controlled application of deformations.

6. Temperature measurements

To illustrate the principle of the measurement, Fig. 4 presents the evolution of the trace at given positions when the FUT experiments a local temperature change. The figure was obtained with the $Chirp_3$ frequency profile, showing a total spectral content of 2.32 GHz. For this demonstration, heat was aplied in the last 20 m of the 1 km FUT, while the remaining FUT was keep at the same temperature. Traces were acquired with a frequency of 1 Hz, without averaging. As expected, the trace remained the same outside the heated point, but started to shift longitudinally in the the last 20 m. In Fig. 4(a) (non heated region) it can be observed that the three consecutive traces remain constant over the time. In contrast, in Fig. 4(b) (heated region) it is possible to observe a longitudinal shift of the trace. The traces are separated by around 17 samples each with 40 GHz sampling rate, i.e., 425 ps. This corresponds to an approximate variation of $\approx 8 \cdot 10^{-3}$ °C in temperature from trace to trace (in agreement with the expectation), which gives us an idea of the potential of this system for high resolution measurements.

#259636 Received 18 Feb 2016; revised 22 May 2016; accepted 23 May 2016; published 7 Jun 2016

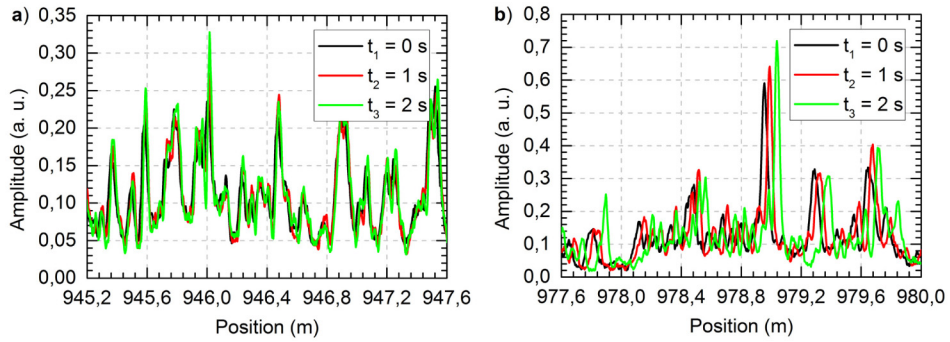

Fig. 4. Longitudinal shift of the ΦOTDR trace when temperature changes are applied to the FUT. a) Non heated region; b) Heated region.

As it was demonstrated in Eq. (5), the longitudinal shift for a given refractive index change ($\Delta n/\Delta t$) depends on the chirp slope ($\delta v/\tau_p$) used. To experimentally demonstrate this principle, a controlled temperature variation of 5 °C was applied on the same point employing the three different chirp slopes. The results are shown in Fig. 5. For the same temperature changes, the observed longitudinal shifts are inversely proportional to the chirp slope, as expected. This principle allows for the sensitivity of the sensor to be tuned by acting on the chirp of the interrogating pulses. Using Eq. (5) and 7, the total temperature change was calculated for each chirp: $\Delta T_{Chirp1} = 4.957$ °C, $\Delta T_{Chirp2} = 5.005$ °C, $\Delta T_{Chirp3} = 5.116$ °C. These are therefore in agreement with the temperature change of 5 ± 0.1 °C recorded by a manual thermometer with 0.1 °C resolution. Note that the temperature variations correspond to a frequency shift of ≈6.7 GHz (Eq. (7), which exceeds the pulse spectral content in all three cases.

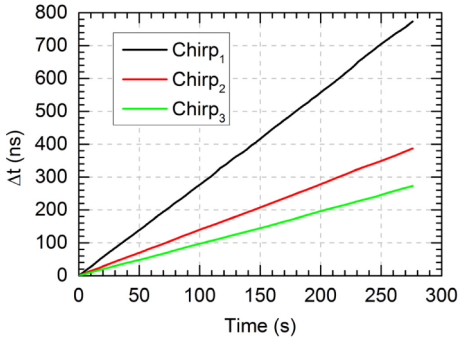

Fig. 5. Longitudinal trace shifts correspondent to a linear temperature variation of 5 °C applied over 280 s for the three different pulse chirp slopes shown in Fig. 3 of meter 979.

To evaluate the long term stability of the sensor, the last 20 m of the FUT were heated from 23 °C to 27.5 °C and cooled to the starting temperature, over approximately 270 minutes, while the entire FUT was monitored. Figure 6(a) shows the temperature evolution of the meter 979 of the FUT – the center of the heated section. The black line represents the fiber temperature measured with the ΦOTDR, while the green dots are the thermometer measurements (green lines represent the measurement error of the thermometer). As it is observed, the fiber follows perfectly the temperature variations with a negligible accumulated error. Finally, Fig. 6(b) shows the temperature profile along 70 m of fiber around the heated section at different times. The heated section is perfectly detected by the system which has enough spatial resolution (10 m) to observe a heated section of 20 m. As expected, in the regions outside the heatead section (which were keept at constant temperature), the ΦOTDR sensor recorded a constant temperature with no variations over time.

#259636 Received 18 Feb 2016; revised 22 May 2016; accepted 23 May 2016; published 7 Jun 2016

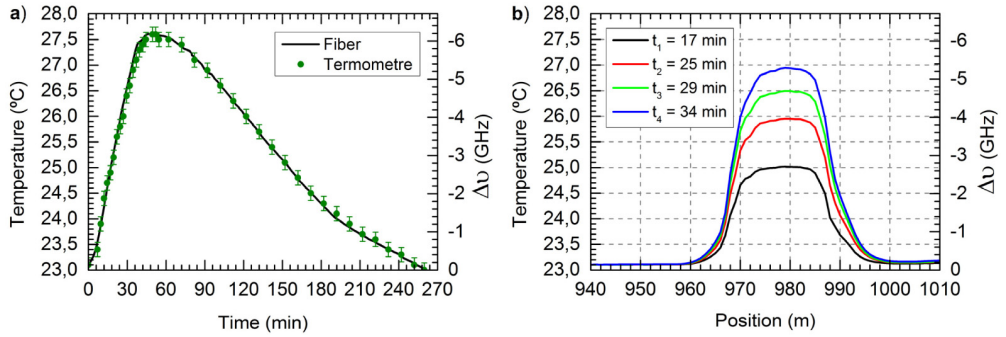

Fig. 6. Measured temperature variations when temperature is raised from 23 °C to 27.5 °C and back to 23 °C in 20 m of fiber around meter 979 of the FUT, over 270 minutes. (a) Temperature evolution of meter 979 along time (b) Temperature profile along 70 m of fiber at different times.

7. Strain and vibrations measurements

After the temperature measurements, the feasibility of the proposed sensor for dynamic and static strain measurements was analysed. As in the previous section, 100 ns optical pulses with a spectral content of $Chirp_3$ = 2.32 GHz were used to realize the measurements.

Firstly, the stability of the sensor over several minutes for large applied strains was analysed. For this, deformations were applied by manually acting on a linear translation stage to which a fiber section near the end of the FUT was glued. The ΦOTDR traces were acquired with a frequency of 2 kHz and the total measured strain was calculated by integrating the strain variations measured from trace to trace. Figure 7 presents the strain variations measured by the ΦOTDR when deformations correspondent to strains varying from 0 με to ± 300 με and back to 0 με were applied. Note that the total frequency shift correspondent to 300 με is ≈45.4 GHz (Eq. (6), and that the total integrated strain variation applied was 1200 με (≈181.4 GHz), which largely exceeds the pulse spectral content (2.32 GHz). However, the calculated strain was observed to return to zero when the applied strain was returned to zero after 160 s. This again clearly demonstrates the long term stability of the sensor and that large measurement ranges (which largely exceed the equivalent to the pulse spectral content) are achievable.

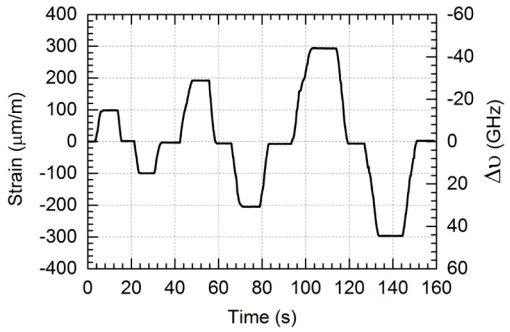

Fig. 7. Measured strain variations when strain applied to the fiber is manually varied (using a linear translation stage) from 0 με to ± 300 με and back to 0 με, near the end of the FUT, over 160 seconds.

In order to characterize the dynamic strain sensing capability of the sensor, the last 20 m of the FUT were strapped around a PZT, which applied deformations controlled by an electrical input. The ΦOTDR traces were now acquired with a frequency of 4 kHz.

#259636 Received 18 Feb 2016; revised 22 May 2016; accepted 23 May 2016; published 7 Jun 2016

The dynamic strain measurements are presented in Fig. 8. Figure 8(a) presents the measured strain when a 1 Hz sinusoidal strain is applied to the fiber by the PZT, with a maximum amplitude of 100 nε. As it is clearly observed, a good agreement between the experimental measure and the applied strain is observed. Furthermore, the quantization error (set by the system minimum temporal resolution in determing Δt of 25 ps, i.e., 1 sample at 40 GHz) is clearly observed, thus demonstrating the resolution limit of the system of 4 nε (Eq. (5,6).

It should be mentioned that in this case, the total measured strain was calculated by simply using the strain variations calculated with reference to the first trace of the measurement (at t = 0). This was possible as in the frequency shift (17 MHz) correspondent to the maximum applied strain (± 100 nε) was significantly lower (<1%) than the pulse total spectral content (2.32 GHz) in this case.

Figure 8(b) presents a spectrogram of the frequencies measured by the ΦOTDR when the PZT applied a frequency sweep between the frequencies 450 Hz to 850 Hz with a period of 1 s. The instantaneous frequency of the spectrogram was calculated using a moving window of 40 ms width over the recovered correlation shift profile. The high linearity of the transfer function of the sensor is clearly demonstrated as no harmonics are observed in frequencies of up to 2 kHz. The SNR of the measured frequencies is >25 dB, which clearly indicates the potential of this technique for achieving simultaneously true strain measurements, high linearity and good signal to noise ratio.

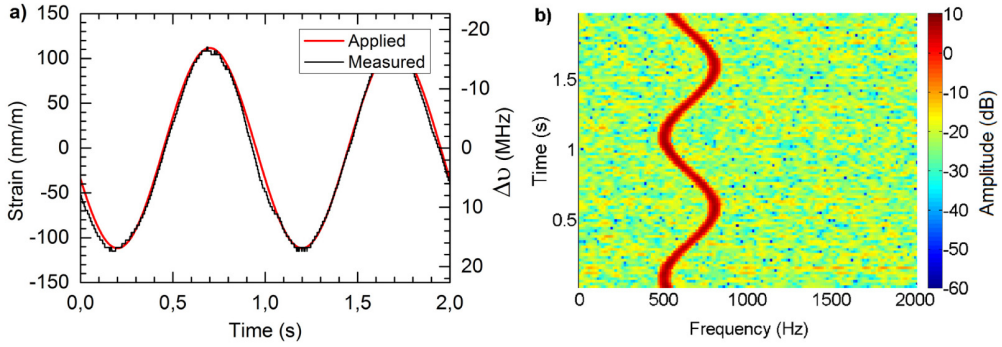

Fig. 8. Measured dynamic strain variations when strain is applied by a PZT in 20 m of fiber around meter 979 of the FUT. a) Measured strain for a 1 Hz sinusoidal strain with 100 nε maximum amplitude. (b) Spectrogram (logarithmic scale - dB) for an applied strain of a frequency sweep between 450 Hz to 850 Hz with a period of 1 s (instantaneous frequency calculated using a moving window of 40ms width of the measured dynamic strain).

8. Conclusions

In this work, a simple and innovative distributed fiber sensor for dynamic measurement of temperature and strain variations was presented. It is based on ΦOTDR using linearly chirped pulses. The system avoids the need of performing laser frequency sweeps, replacing them by the computation of simple correlations from trace to trace. It also avoids the use of complex and un-stable phase recovery techniques relying on a local oscillator. The resolution of the sensor can be tuned by acting on the pulse chirp slope. With simple setups, temperature/strain resolutions of 1mK/4nε could be readily demonstrated. It was also shown that the sensing method can cumulatively track large total temperature/strain variations (much larger than those equivalent to the total spectral content of the pulse), as long as the variations from trace to trace are small enough and care in the processing is taken so as to keep the cumulative errors bounded. The system allows for the precise quantification of temperature/strain change variations in a single shot, reaching measurement speeds at kHz rates, while maintaining reliability over several hours. A conceptual demonstration with a spatial resolution of 10 m over 1 km is provided, but the system should in principle allow for similar settings to

#259636 Received 18 Feb 2016; revised 22 May 2016; accepted 23 May 2016; published 7 Jun 2016

traditional ΦOTDR, with metric spatial resolutions over tens of kilometers. The presented sensor has potential to greatly extend the operating ranges of ΦOTDR. The only cost increase of the sensor appears in the detection scheme and in the digitizer, both of which scale with the amount of chirp applied. For the typical settings used in our experiments, sampling speeds of several GHz should indeed be necessary with correspondingly high photodetection bandwidths. Still, the system proves to be far more simple and robust than other dynamic and distributed strain/temperature measurement methods reported in the literature. Further work on the limitations of the system (specially for long measurement ranges) should be done, particularly those related to the fiber chromatic dispersion.

Acknowledgments

This work was supported by the European Research Council (ERC) through Starting Grant UFINE (Grant no. 307441), the Spanish MINECO through project TEC2013-45265-R, and the regional program SINFOTON-CM S2013/MIT-2790. Juan Pastor-Graells acknowledges funding from the Spanish MINECO through a FPI contract. Hugo F. Martins acknowledges EU funding through the FP7 ITN ICONE program, gr. #608099. Sonia Martin-Lopez acknowledges funding from the Spanish MINECO through a "Ramon y Cajal" contract.

#259636 Received 18 Feb 2016; revised 22 May 2016; accepted 23 May 2016; published 7 Jun 2016